



Ameliorative effect of total ginsenosides from heat-treated fresh ginseng against cyclophosphamide-induced liver injury in mice

Ping Tang^{a,b,1}, Guangquan Ren^{a,b,c,1}, Hongyang Zou^{a,b}, Sitong Liu^{a,b}, Junshun Zhang^{a,b}, Zhiyi Ai^{a,b}, Yue Hu^{a,b}, Linlin Cui^{a,b}, Bo Nan^{a,b}, Zhicheng Zhang^{b,c,**}, Yuhua Wang^{a,b,*}

^a College of Food Science and Engineering, Jilin Agricultural University, Changchun, China

^b Jilin Province Innovation Center for Food Biological Manufacture, Jilin Agricultural University, Changchun, China

^c International Football Education School, Jilin Agricultural University, Changchun, China

ARTICLE INFO

Keywords:

Ginseng
Heat treatment
Total ginsenoside
Cyclophosphamide
Liver injury

ABSTRACT

This study evaluated the effect of heat treatment on the conversion of ginsenoside and the ameliorative effect of heat-treated total ginsenoside (HG) from fresh ginseng on cyclophosphamide (CTX)-induced liver injury. LC-MS analysis revealed that the content of rare ginsenosides increased markedly after heat treatment. HG significantly attenuated CTX-induced hepatic histopathological injury in mice. Western blotting analysis showed that untreated total ginsenoside (UG) and HG regulated the Nrf2/HO-1 and TLR4/MAPK pathways. Importantly, these results may be relevant to the modulation of the intestinal flora. UG and HG significantly increased the short-chain fatty acids (SCFAs)-producing bacteria *Lactobacillus* and reduced the LPS-producing bacteria *Bacteroides* and *Parabacteroides*. These changes in intestinal flora affected the levels of TNF- α , LPS and SCFAs. In short, UG and HG alleviated CTX-induced liver injury by regulating the intestinal flora and the LPS-TLR4-MAPK pathway, and HG was more effective. HG has the potential to be a functional food that can alleviate chemical liver injury.

1. Introduction

Cyclophosphamide (CTX), a broad-spectrum alkylated anticancer drug, is widely used to treat malignant tumors. CTX kills fast-growing tumor cells by damaging DNA and, at the same time, kills healthy cells that normally proliferate in the body, such as liver cells and intestinal epithelial cells (N. Zhang et al., 2022). The liver is the main metabolic site for CTX, which leads to liver injury and apoptosis by triggering oxidative stress (Z. Zhang et al., 2020). The gut plays an important role in protecting the body from exogenous infections. The intestinal barrier is a key factor in ensuring intestinal health. The intestinal tract contains massive bacteria that interact with each other in

the gut to form a balanced micro-ecosystem that constitutes a microbial barrier (Su et al., 2023). As CTX indiscriminately damages self-renewing intestinal epithelial cells, leading to damage to the intestinal barrier and an increase in intestinal permeability, the distribution and composition of the intestinal flora is also altered (Zhao et al., 2020). The intestine and liver interact with each other due to the presence of the enterohepatic axis (Wu et al., 2020). When the liver is damaged, the intestinal microbial composition and the integrity of the intestinal epithelial cells are disrupted. And the abnormal changes in the intestinal microbiota can lead to damage of the intestinal barrier, and the LPS released from the surface of gram-negative bacteria in the intestines leaks and enters the liver through the portal vein, which in turn causes liver injury. Hong

Abbreviations: AKT, protein kinase B; ALT, alanine aminotransferase; AST, aspartate aminotransferase; BW, body weight; CTX, cyclophosphamide; ERK, extracellular signal-regulated protein kinase; GSH, glutathione; GSH-Px, glutathione peroxidase; H&E, hematoxylin and eosin; HO-1, heme oxygenase 1; JNK, c-Jun N-terminal kinase; MAPKs, mitogen-activated protein kinases; MDA, malondialdehyde; Nrf2, nuclear factor erythroid 2-related factor 2; PMSF, phenylmethanesulfonyl fluoride; PVDF, polyvinylidene fluoride; RIPA, radioimmunoprecipitation assay; SDS-PAGE, sodium dodecyl sulfate-polyacrylamide gel electrophoresis; SPF, specific pathogen-free; T-SOD, total superoxide dismutase.

* Corresponding author. College of Food Science and Engineering, Jilin Agricultural University, Changchun, China.

** Corresponding author. International Football Education School, Jilin Agricultural University, Changchun, China.

E-mail addresses: 1536255183@qq.com (P. Tang), 15643186667@163.com (G. Ren), 1322202217@qq.com (H. Zou), 3037989799@qq.com (S. Liu), zhangjunshun01@163.com (J. Zhang), azy1112@163.com (Z. Ai), hy20191007@163.com (Y. Hu), 1871949344@qq.com (L. Cui), nanbo@jlau.edu.cn (B. Nan), zhangzhicheng3777@jlau.edu.cn (Z. Zhang), yuhua-ww@163.com (Y. Wang).

¹ Made the same contribution as the first author.

<https://doi.org/10.1016/j.crf.2024.100734>

Received 29 December 2023; Received in revised form 15 March 2024; Accepted 6 April 2024

Available online 17 April 2024

2665-9271/© 2024 The Authors. Published by Elsevier B.V. This is an open access article under the CC BY-NC license (<http://creativecommons.org/licenses/by-nc/4.0/>).

et al. found that CTX disrupted the intestinal flora composition and intestinal permeability in mice, and significantly increased the number of LPS-producing bacteria, leading to massive LPS entry into the liver through the portal vein, resulting in liver inflammation and injury (Hong et al., 2022). Similarly, Li et al. found that CTX caused liver injury by disrupting the intestinal microbial balance and affecting intestinal metabolic functions (X. Li et al., 2023). Since CTX has non-negligible toxic side effects, seeking a means to mitigate CTX-induced liver injury is important for the physical and mental health of chemotherapy patients. Therefore, maintaining gut microbiome homeostasis may be an important strategy to mitigate CTX-induced liver injury.

Various methods, such as Mesna (antioxidants), Ondansetron, the use of low-dose CTX in combination with other anticancer drugs, and the application of CTX analogs, have been adopted to mitigate the toxic side effects of CTX (Patwa et al., 2020). However, due to the limitations in the application of chemical-based drugs, natural and safe functional ingredients of plant origin have gained extensive attention from scholars in the food and pharmaceutical industries. Ginseng (*Panax Ginseng* C.A. Meyer) is a perennial herb, that has been utilized for thousands of years as an important health food ingredient worldwide (Song et al., 2023). A previous study reported that ginseng may act as a hepatoprotector against CTX-induced liver injury (Abdelfattah-Hassan et al., 2019). Ginsenoside is the most important bioactive component in ginseng (K. Li et al., 2019). The ginsenosides with a relatively high percentage in natural ginseng are referred to as major ginsenosides, while ginsenosides with low percentages are called rare ginsenosides (J. Zhang et al., 2022). Notably, rare ginsenosides have better bioavailability and transmembrane permeability than major ginsenosides due to their smaller size (Ms et al., 2018). Currently, several methods for increasing the bioactivity of ginseng through the conversion of ginsenosides have been developed, such as physical, chemical and biological methods. However, physical transformation is more conducive for application in factories than other methods. There are reports that rare ginsenosides Rg3, Rh2 and Rk3 ameliorated acetaminophen-induced hepatotoxicity (Gao et al., 2021), cyclophosphamide-induced immune deficiency (Y. Qian et al., 2019), and hepatic non-alcoholic lipid inflammation (Guo et al., 2023). Chen et al. reported that total ginsenosides were highly effective at improving CTX-induced liver injury (J et al., 2021). Xue et al. reported that the crude ginsenosides from *Panax quinquefolius* were treated at 130 °C for 3 h to gain heat-converted ginsenosides which had a relatively stronger antibacterial effect (Xue et al., 2017). Total ginsenosides treated at 80 °C and 75% relative humidity for 12 days had greater cytotoxic effects on HepG2 cells than did untreated total ginsenosides (R. Liu et al., 2022). However, there are very few studies on the ameliorative effects of heat-treated total ginsenosides from fresh ginseng on liver injury induced by CTX and the mechanism of the ameliorative effects is unclear.

The current research optimized the conditions for the conversion of rare ginsenosides by heat treatment and further evaluated the effects of total ginsenosides from heat-treated fresh ginseng on CTX-induced liver injury. This research demonstrated that HG ameliorated CTX-induced liver injury through the Nrf2/HO-1 and TLR4/MAPK pathways. Moreover, the regulatory effects of HG on SCFAs and the composition of gut microbiota were evaluated. This work may contribute to the theoretical evidence and reference value for the development of ginsenosides as functional foods with the ability to mitigate chemotherapeutic injury.

2. Material and methods

2.1. Material and reagents

5-year-old cultivated fresh ginsengs were obtained from Jingyu County, Jilin Province, China. The ginsenosides PPD, Rb1, Rf, F2, Rg3, Rh1, Ro, Rc, Rb2, Rg1, Re, Rf, Rh2 and oleanolic acid (OA) were ordered from Nanjing Jingzhu Biotechnology Corporation, China. Acetonitrile, methanol and formic acid (HPLC ≥98%) were purchased from Merck

(Germany). CTX was bought from Shanghai Yuanye Bio-Technology Corporation (Shanghai, China). Commercial kits for alanine aminotransferase (ALT), aspartate aminotransferase (AST), hydroxyl free radical assay kit, glutathione peroxidase (GSH-Px), glutathione (GSH), malondialdehyde (MDA), and total superoxide dismutase (T-SOD) were provided from Nanjing Jian Cheng Bioengineering Inc. (Nanjing, China). Radioimmunoprecipitation assay (RIPA, 89900) and phenylmethanesulfonyl fluoride (PMSF, 36978) buffer were bought from Thermo Fisher Scientific (MA, USA). The primary antibodies of c-Jun N-terminal kinase (JNK), p-JNK, extracellular signal-regulated protein kinase (ERK), p-ERK, p38, p-p38, toll-like receptor 4 (TLR4), heme oxygenase 1 (HO-1), Nrf2, the secondary antibodies of HRP-labeled goat Anti-Rabbit IgG H&L (ab205718, 1:5000) and HRP-labeled goat Anti-Mouse IgG H&L (ab6789, 1:5000) and β-actin (ab8226, 1:2000) antibodies were ordered from Abcam (Cambridge, UK). Other reagents (analytical grade) were ordered from standard commercial suppliers.

2.2. Preparation of total ginsenosides

Fresh ginsengs of the uniform thickness and size were selected, cleaned, and then put into a homogenizer to prepare ginseng pulp. Fresh ginseng pulp was heat-treated according to the optimal heat-treatment conditions screened in previous laboratory studies (135 °C, 30 min, 103 kPa, 60 mM citric acid). The fresh ginseng pulp and heat-treated ginseng pulp were freeze-dried, 1.0 g of freeze-dried ginseng powder was weighed precisely, and the fat was removed by heating and refluxing with petroleum ether for 3 h in the Soxhlet extraction device. The filter cartridges were placed in a fume hood to evaporate dryness. The evaporated dry powder was immersed in 50 mL of water-saturated n-butanol solution and then sealed and left to stand overnight; it was ultrasonicated for 30 min, after which the filter solution was measured precisely and subsequently dried in 25 mL of the filter solution. UG and HG were the total ginsenosides from the untreated and heat-treated fresh ginseng, respectively (purity of 90–93%).

2.3. Determination of the total ginsenoside content

The ginsenoside content was detected by vanillin-sulfuric acid colorimetry. Briefly, 100 μL of the extract, 5 mL of 72% sulfuric acid solution and 0.5 mL of 8% vanillin-ethanol solution were stirred together in a test tube and then subjected to incubation at 60 °C in a water bath for 10 min, followed by incubation in a cold-water bath for 10 min. The absorbance was determined at 544 nm using ginsenoside Re as the standard. The standard curve was evaluated as $y = 0.0021x - 0.0016$ ($R^2 = 0.9998$).

2.4. Analysis of ginsenosides

The qualitative and quantitative analysis of total ginsenosides from fresh ginseng was accomplished by high-performance liquid chromatography-mass spectrometry (LC-MS). The HPLC system (Ulti-Mate 3000, THERMO) was fitted with a C18 column (ACQUITY UPLC HSS T3, Waters, 2.1 × 100 mm, 1.8 μm). The column temperature was kept at 40 °C, and the loading volume was 3 μL. The mobile phase consisted of A: 0.1% formic acid water and B: 0.1% formic acid acetonitrile using a binary gradient elution of 5%–10% at 0–5 min, 10%–40% at 5–34 min, 40%–95% at 34–57 min, 95%–5% at 57–60 min. The flow rate and the injection volume were 400 μL/min and 3 μL. MS analysis of ginsenosides was performed on the AB X500R Triple TOF mass spectrometer. The molecular ions with the strongest strength and greater than 100 were selected for collection of secondary mass spectrometry data in each data collection cycle. The primary acquisition range was 50–1200, 10 secondary spectra were acquired every 50 ms, and the bombardment energy was 30 eV. The ESI Ion Source parameters are configured as follows: atomization pressure (GS1) and auxiliary pressure: 60 Psi, spray voltage: 5000 V (positive ion mode), air curtain

pressure: 35 Psi, temperature: 650 °C.

2.5. Animals and experimental design

Forty male SPF BALB/c mice (5–6 weeks old, 20 ± 2.0 g) were purchased from Changsheng Biotechnology corporation (Liaoning, China). All the experimental procedures concerning the animals and their caring were authorized by the Animal Ethics Committee of Jilin Agricultural University (No. 20190410005). All mice were allowed to acclimatize to a controlled environment for 7 days (12 h light/dark cycle, free access to food and water, 25 ± 1 °C, 40–55% relative humidity) and randomized to four groups: NC (normal control group), MC (CTX control group), UG (CTX + 40 mg/kg total ginsenosides from fresh ginseng) and HG (CTX + 40 mg/kg total ginsenosides from heat-treated fresh ginseng). While the NC group was intraperitoneally (i.p.) injected with saline, the other groups were injected with 40 mg/kg body weight (BW)/d CTX (diluted in saline) for 3 days. After the model was established, the four groups of mice were given fixed doses of saline, UG or HG by gavage. The detailed design of the animal testing procedure is shown in Fig. 2A. Mice were fasted for 12 h and anesthetized for euthanasia. All the mice were weighed daily during the experiment. Before sacrificing the animals, fecal samples were collected. Blood samples were collected from the orbital vascular plexus, allowed to stand for 4 h, and centrifuged at 4 °C and 3000 rpm for 20 min to separate the serum. The cecal contents were gathered and liver tissues were weighed. All the samples were immediately stored at -80 °C until further analysis. The liver indices were calculated according to the formula: [liver weight (mg)/body weight (g)].

2.6. Histological analysis

The liver tissues were fixed with 4% paraformaldehyde (Absin, Shanghai, China) for more than 24 h and then paraffin-embedded. Successive 5- μ m-thick sections were used for hematoxylin and eosin (H&E) staining. Finally, the tissue segments were observed using a light microscope (Leica, Germany), and images were captured (100 \times and 400 \times).

2.7. Biochemical analysis

The liver tissues were homogenized (10%, w/v) in 50 mM cold phosphate buffer (pH 7.4) and centrifuged (4 °C, 2500 rpm, 10 min), after which the supernatant was collected for determination of enzyme activity. The levels of ALT, AST, GSH, GSH-Px, MDA and T-SOD in the liver and serum were measured using commercial assay kits, and the cytokine TNF- α was measured using ELISA kits. LPS in the liver or serum was measured using endotoxin detection kits. All data were measured by a multimode plate reader (PerkinElmer, USA).

2.8. Western blot analysis

Liver tissue protein from the mice was extracted from the mice with RIPA buffer, phosphatase inhibitor and PMSF protein inhibitor (98:1:1) for 20 min on ice, followed by centrifugation for supernatants (4 °C, 12,000 rpm, 20 min). The protein concentration was measured using a BCA protein quantification kit (Beyotime, Shanghai, China), and the proteins were separated by 8% or 10% (w/v) sodium dodecyl sulfate-polyacrylamide gel electrophoresis (SDS-PAGE) and transferred onto polyvinylidene fluoride (PVDF) membranes. The PVDF membranes were blocked with QuickBlock™ Blocking Buffer (Beyotime, Shanghai, China) for 15 min at room temperature. After incubating the above PVDF membranes with the corresponding primary and secondary antibodies, the target proteins were visualized using a chemiluminescence (ECL) system through an image scanner (iBright CL1000, Thermo Fisher Scientific, USA). Protein levels were normalized to the corresponding β -actin expression and the band intensities were quantified by ImageJ

software (The National Institutes of Health, USA).

2.9. Measurement of SCFAs in mice feces

100 mg feces of mice were taken, and added with phosphoric acid solution (0.5% v/v), vortexed thoroughly, and sonicated at 4 °C for 10 min. 500 μ L of MTBE solvent containing the internal standard was added and vortexed for 3 min. After sonication for 5 min in an ice water bath, centrifuged at 12000 r/min at 4 °C for 10 min. Then, 200 μ L of the supernatant was transferred to an injection vial for GC-MS/MS analysis.

2.10. 16S rRNA sequencing of the cecal contents of the gut microbiota

Total genomic DNA was extracted from cecal content samples following the OMEGA Soil DNA Kit (M5635-02) (Omega Bio-Tek, Norcross, GA, USA), and the DNA extraction was measured using a Nano-Drop NC2000 spectrophotometer (Thermo Fisher Scientific, Waltham, MA, USA) and agarose gel electrophoresis. The primers 338F (5'-ACTCCTACGGGAGGCAGCA-3') and the reverse primer 806R (5'-GGACTACHVGGGTWTCTAT-3') were used to amplify the V3–V4 region of the bacterial 16S rRNA genes via polymerase chain reaction (PCR). PCR amplifications were purified with Vazyme VAHTSTM DNA Clean Beads (Nanjing, China) and quantified using the Quant-iT PicoGreen dsDNA Assay Kit (Invitrogen, Carlsbad, CA, USA). After the separate quantification steps, amplicons were pooled in equal amounts and sequenced in pairs of 2×250 bp using the Illumina MiSeq platform with the MiSeq Reagent Kit V3 at Shanghai Personal Biotechnology (Shanghai, China).

2.11. Statistical analysis

The data in Fig. 2B and C were analyzed by two-way ANOVA, and the remaining data were analyzed by one-way ANOVA (GraphPad Prism 8.0.2 software, USA). The Data were expressed as the mean \pm SD. The statistical significance of the differences between groups was determined by Tukey's multiple comparison test. Differences were considered to be statistically significant at $p < 0.05$.

3. Results

3.1. The effect of heat treatment on the ginsenosides from fresh ginseng

The contents of ginsenosides in untreated fresh ginseng and heat-treated fresh ginseng were 49.43 ± 4.23 mg/g, 54.62 ± 5.88 mg/g, respectively (Fig. 1A). The total ginsenosides from heat-treated fresh ginseng were quantitatively analyzed via LC-MS (Fig. 1B). The major ginsenosides Ro, Rb1, Rb2, Rb3, Rc, Rd, Re, Rf, Rg1, and Rg2 were 3.294 mg/g, 0.675 mg/g, 0.942 mg/g, 1.014 mg/g, 1.025 mg/g, 0.468 mg/g, 0.217 mg/g, 0.699 mg/g, 0.430 mg/g and 0.070 mg/g, the rare ginsenosides Rg3, Rh2, Rk1, Rg5 and CK were 0.080 mg/g, 0.002 mg/g, 0.058 mg/g, 0.011 mg/g and 0.025 mg/g in fresh ginseng. While in heated fresh ginseng, the major ginsenosides Ro, Rb1, Rb2, Rb3, Rc, Rd, Re, Rf, Rg1, and Rg2 contents were 0.142 mg/g, 0.011 mg/g, 0.005 mg/g, 0.005 mg/g, 0.005 mg/g, 0.041 mg/g, 0.008 mg/g, 0.037 mg/g, 0.005 mg/g and 0.044 mg/g, and the rare ginsenosides Rg3, Rh2, Rk1, Rg5 and CK contents were 0.564 mg/g, 0.212 mg/g, 0.832 mg/g, 0.771 mg/g and 0.067 mg/g. Importantly, two ginsenosides, Rk2 and Rh3, were not present in untreated fresh ginseng, and their contents were 0.110 mg/g and 0.096 mg/g. Moreover, the possible conversion paths of PPD-type and PPT-type ginsenosides in heat-treated fresh ginseng were summarized in Fig. 1C and D. The conversion pathways are as follows: Rb1, Rb2, Rb3 \rightarrow Rc \rightarrow Rd \rightarrow Rg3 \rightarrow Rh2 \rightarrow Rh3; Rb1, Rb2, Rb3 \rightarrow Rc \rightarrow Rd \rightarrow Rg3 \rightarrow Rg5 \rightarrow Rh3; Rb1, Rb2, Rb3 \rightarrow Rc \rightarrow Rd \rightarrow Rg3 \rightarrow Rk1 \rightarrow Rk2; Re \rightarrow Rg1 \rightarrow F1; and Re \rightarrow Rg2 \rightarrow Rh1.

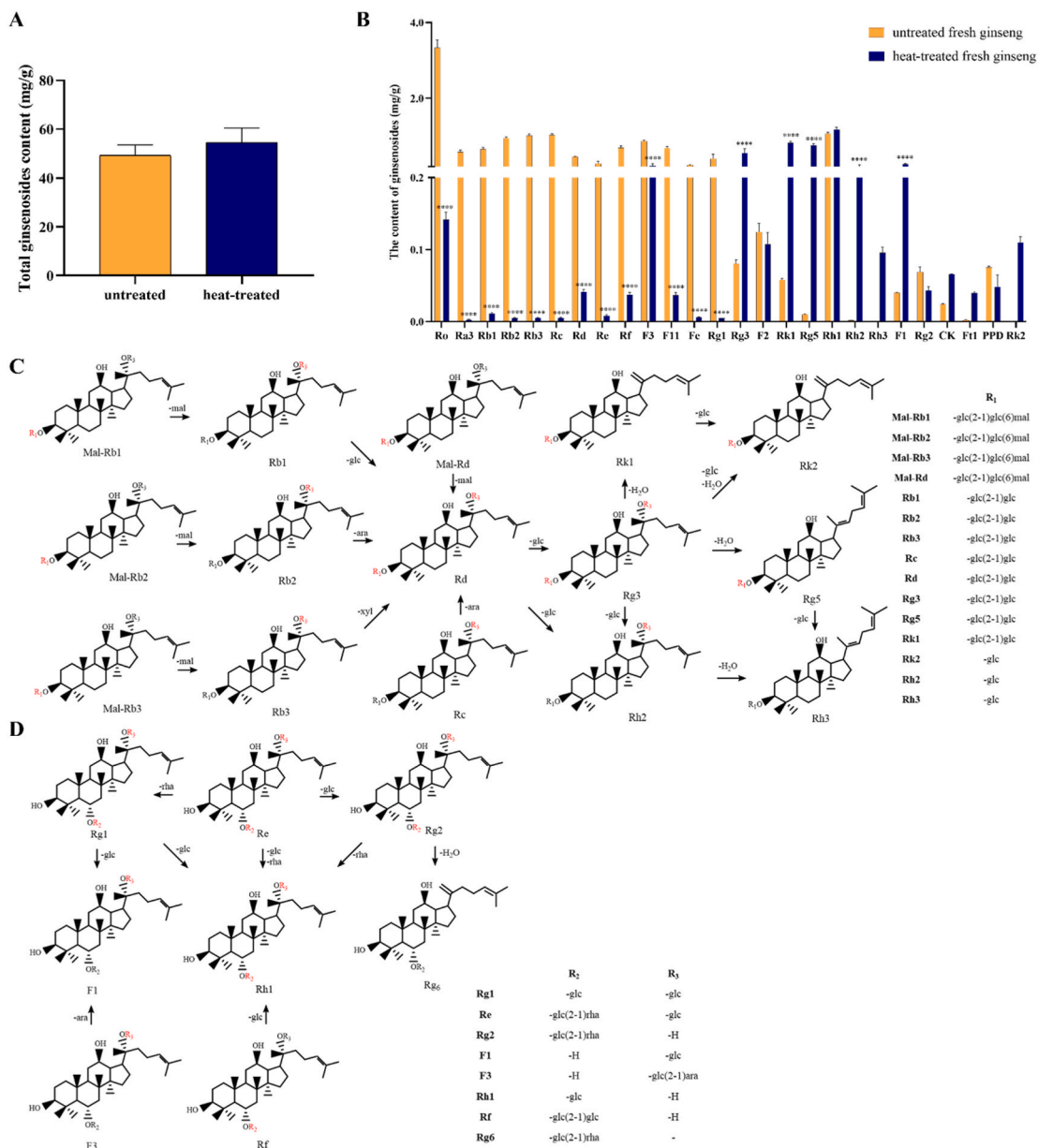


Fig. 1. Effect of heat treatment on ginsenosides from fresh ginseng. (A) The content of total ginsenosides in the untreated and heat-treated fresh ginseng; (B) Changes in the content of each ginsenoside in the untreated and heat-treated fresh ginseng; Diagram of possible transformation pathways of (C) PPD-type ginsenosides; (D) PPT-type ginsenosides during heat treatment. Data were shown as mean ± SD (n = 3). (**p* < 0.01), (***p* < 0.001), (***)*p* < 0.0001) as compared to the UG.

3.2. Effects of HG on body weight, daily intake and liver indices in CTX-induced mice

The NC group mice had a regular increase in body weight and food intake (Fig. 2A–C). However, the MC group mice developed severe anorexic behaviors and had a significant decrease in body weight and food intake after treatment with CTX (*p* < 0.001), which was consistent with the clinical performance of chemotherapy patients taking CTX for long periods of time. However, the mice recovered better after intervention with UG or HG, which effectively alleviated the CTX-induced reduction in body weight and food intake. The liver indices were significantly greater in the MC group than in the NC group (*p* < 0.05), indicating liver damage. However, intervention with UG or HG reversed these changes (*p* < 0.01) (Fig. 2D).

3.3. Effect of HG on hepatic damage in CTX-induced mice

As shown in Fig. 3A, significant lesions, such as whitening and swelling were observed in the livers of the MC group mice compared to the NC group mice. After intervention with UG or HG, the liver tissue morphology of mice was significantly better. In addition, the H&E staining results again confirmed the above viewpoints (Fig. 3B). The liver sections of the NC group mice exhibited normal liver lobule structures with clear boundaries, and the hepatocytes were arranged radially with the central vein. The MC group mice had abnormal hepatocyte structures, turbid liver cords and sinusoids, swollen hepatocytes with fragmented nuclei, and congestion of the central vein and hepatic sinusoids, as indicated by the red arrows in the figure; these changes were accompanied by massive infiltration of inflammatory cells as shown by the red circles. After the intervention with UG and HG, the

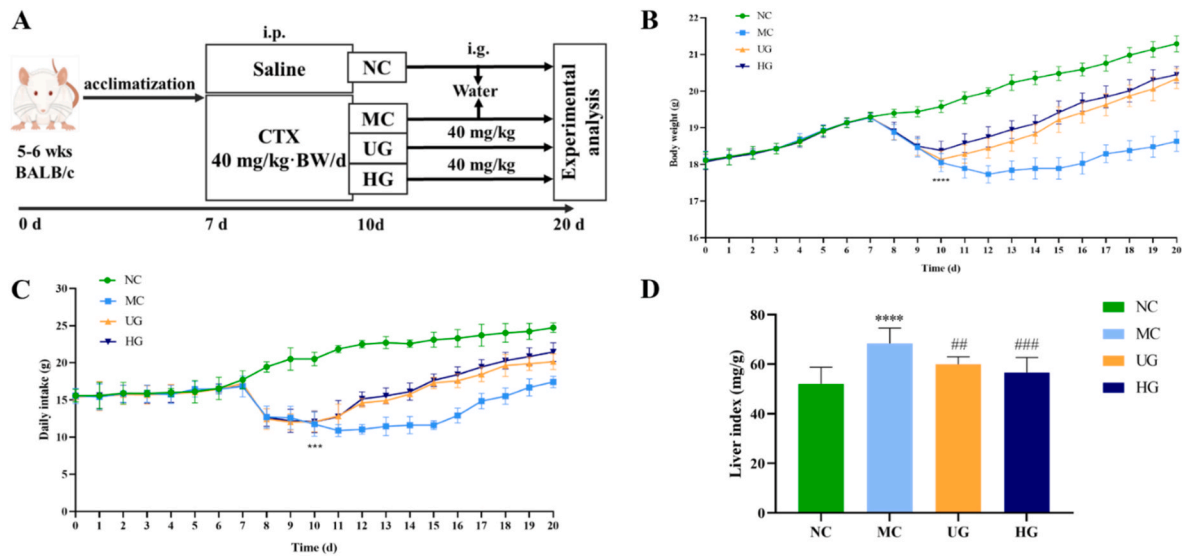


Fig. 2. Effect of HG on liver injury in mice induced by CTX. (A) The animal experimental procedure; (B) body weight; (C) food intake; (D) liver index. Data were shown as mean ± SD (n = 10). (***p* < 0.001), (*****p* < 0.0001) as compared to the NC group. (#*p* < 0.01), (###*p* < 0.001) as compared to the MC group.

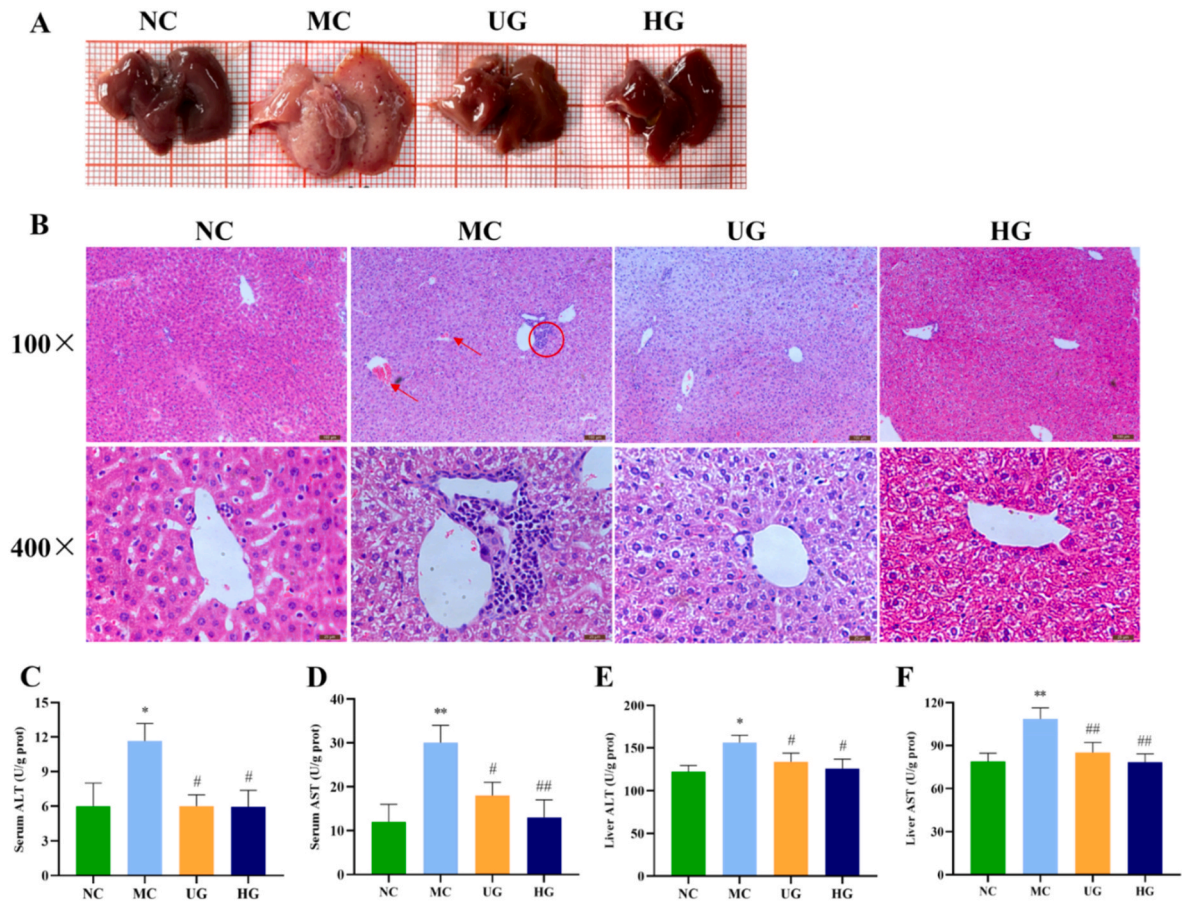


Fig. 3. Effect of HG on hepatic damage in mice induced by CTX. (A) Typical macroscopic photo of the surface of the liver; (B) H&E staining images (100 × and 400 ×, scale bars at 100 μm and 25 μm); (C) Serum ALT; (D) Serum AST; (E) Liver ALT; (F) Liver AST. Data were shown as mean ± SD (n = 10). (**p* < 0.05), (***p* < 0.01) as compared to the NC group. (#*p* < 0.05), (##*p* < 0.01) as compared to the MC group.

structure and arrangement of the hepatocytes were restored, and the hepatic sinusoidal space became clearer. Interestingly, HG improved the CTX-induced pathological disorganization of the mice liver more significantly. Compared with the NC group mice, the serum and liver

ALT and AST levels were significantly higher in the MC group mice (*p* < 0.05) (Fig. 3C–F). ALT and AST levels returned to normal mice level in the UG and HG groups.

3.4. Effects of HG on hepatic oxidative stress in CTX-induced mice

After CTX treatment, there was an increase tendency of the MDA level compared with the normal mice, but no significant difference ($p > 0.05$) (Fig. 4A). The levels of GSH, GSH-Px and T-SOD were significantly reduced in the MC group mice compared with NC group ($p < 0.05$), but the interventions of UG and HG significantly inhibited the reduction in varying degrees, especially HG (Fig. 4B–D). The protein expression levels of Nrf2 and HO-1 were examined to further elucidate the mechanism by which UG and HG intervention enhanced liver antioxidant capacity. CTX significantly inhibited the expression of Nrf2 and its downstream protein HO-1, but UG and HG intervention reversed the changes in the expression of these proteins (Fig. 4E).

3.5. Effects of HG on liver inflammatory mediators and the TLR4/MAPK signaling pathway in CTX-induced mice

The LPS concentration in serum and liver were markedly higher in the MC group than in the NC group ($p < 0.05$), while declined significantly in the HG group ($p < 0.01$) (Fig. 5A–C). The level of TNF- α in the liver was significantly increased in the MC group than in the NC group ($p < 0.01$) and was markedly lower after both the UG and HG interventions ($p < 0.05$) (Fig. 5B–D). The protein expression of the classic LPS receptor TLR4 was significantly greater in the MC group compared with the NC group ($p < 0.05$), and was lower in the UG and HG groups ($p > 0.05$) (Fig. 5E). The three important kinase subfamilies in the MAPK signaling pathway are ERK, JNK and p38, and their activation is marked by phosphorylation. The expression of p-JNK/JNK, p-ERK/ERK, and p-p38/p38 was significantly increased in the MC group mice compared to the NC group mice ($p < 0.05$), suggesting that CTX caused severe hepatic inflammation (Fig. 5E). HG intervention reversed the increase in the phosphorylation of the above proteins ($p < 0.05$).

3.6. Effects of HG on the cecum microbial composition and diversity in CTX-induced mice

As the sequencing depth increased, the rarefaction curve for the cecum contents of the four groups of mice tended to flatten out horizontally. The abundance rank curve spanned horizontally and gradually flattened out in the vertical direction (Fig. 6A and B). The results indicated that the amount of sequencing data was gradual and reasonable, the species composition was rich and evenly distributed, and the sequencing depth was sufficient to represent most of the microbial

diversity information in the all samples.

As shown in Fig. 6C–F, the Chao1, Shannon, Simpson and observed species indices of mice in the MC group were significantly lower than those in the NC group, indicating that CTX altered the diversity and abundance of intestinal microorganisms in mice ($p < 0.05$). The first three indices were markedly greater in the HG group than in the MC group ($p < 0.05$).

PCoA and nonmetric multidimensional scaling (NMDS) analyses were used to characterize the similarity of community structure among different samples. The MC group was clearly separated from the NC group after CTX treatment, which indicated that CTX induced a change in the structure of the gut microbiota in mice (Fig. 6G–H). The UG and HG groups were significantly closer to the NC group, suggesting that UG and HG had ameliorative effects on the intestinal microbial composition of mice.

To identify specific taxa correlated with HG, the relative abundance of the taxa was evaluated at the phylum and genus levels. At the phylum level, the abundance of *Actinobacteria* and *TM7* were significantly lower ($p < 0.05$), and *Proteobacteria* was significantly increased ($p < 0.0001$) in the MC group mice compared to NC group mice. In addition, *Tenericutes* and *Deferribacteres* was reduced significantly after treatment with CTX ($p < 0.0001$). HG intervention significantly reversed these changes ($p < 0.05$), suggesting that HG has a notable effect on the composition of the intestinal flora in mice.

To verify the differences in the gut microbiota among all the groups, the gut microbiota was further analyzed at the genus level. The top 10 microbiotas in terms of relative abundance were showed in Fig. 7B. Compared to the NC group mice, the relative abundance of *Bacteroides*, *[Prevotella]*, *[Ruminococcus]* and *Parabacteroides* was significantly increased ($p < 0.01$) after CTX treatment. However, HG intervention significantly reduced these increases ($p < 0.01$). In addition, the relative abundance of *Lactobacillus* was lower in the MC group than in the NC group ($p < 0.01$), and was significantly increased in the HG treatment group ($p < 0.0001$).

3.7. Effects of HG on SCFA levels in the feces of CTX-induced mice

The impacts of UG and HG on the microbial metabolites in the feces of CTX-induced mice were investigated (Table 1). The contents of acetic acid, butyric acid, valeric acid and total SCFAs in the MC group were lower than the NC group ($p < 0.05$). While the intervention of UG and HG significantly inhibited the CTX-induced decrease in SCFA levels, especially in the HG group. UG and HG promoted the production of

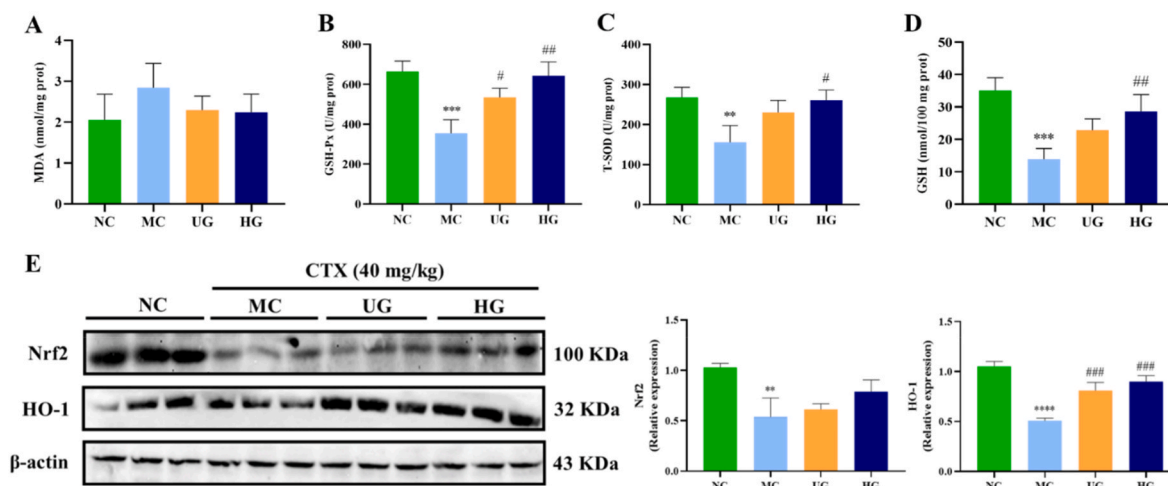


Fig. 4. Effect of HG on the oxidative stress indicator of liver injury induced by CTX in mice. (A) MDA, (B) GSH, (C) GSH-Px, and (D) T-SOD in the liver (E) The relative protein expression of Nrf2 and HO-1. Data were shown as mean \pm SD ($n = 10$). (** $p < 0.01$), (***) $p < 0.001$) and (**** $p < 0.0001$) as compared to the NC group. (# $p < 0.05$), (## $p < 0.01$) and (### $p < 0.001$) as compared to the MC group.

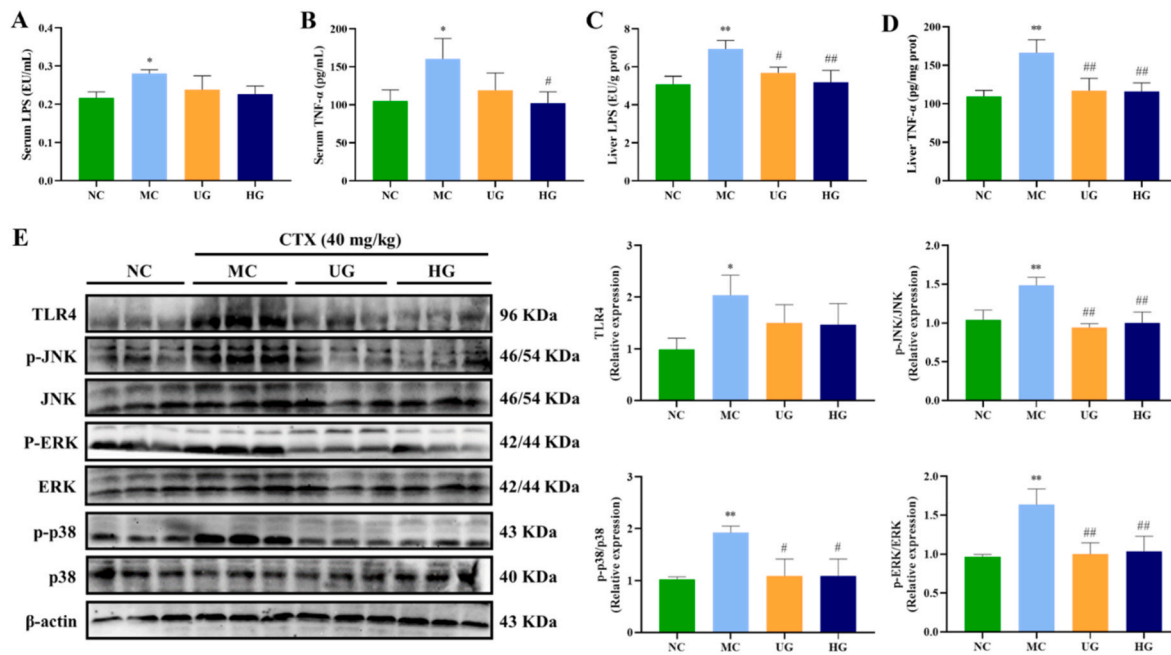


Fig. 5. Effect of HG on inflammatory mediators and the relative expression of the TLR4 signaling pathway in the liver in mice with CTX-induced inflammation. (A) LPS, (B) TNF- α in serum, (C) LPS, and (D) TNF- α in the liver (E) The relative expression of the TLR4 and MAPK (p-JNK/JNK, p-ERK/ERK, p-p38/p38) signaling pathways in the liver. Data were shown as mean \pm SD (n = 10). (* p < 0.05), (** p < 0.01) and (***) p < 0.001) as compared to the NC group. (# p < 0.05), (## p < 0.01) and (### p < 0.001) as compared to the MC group.

SCFAs and exerted beneficial effects.

3.8. The correlation between liver injury-related indicators and key gut microbial taxa

The relationship between differential flora and liver injury-related indicators was determined by Spearman correlation analysis. The abundance of *Lactobacillus* was negatively correlated with the levels of LPS in liver and TNF- α in serum (p < 0.05), but was positively correlated with the levels of acetic acid, propionic acid and butyric acid (p < 0.01) (Fig. 8). The concentration of LPS in the liver had positive correlations with the abundance of *[Prevotella]*, *[Ruminococcus]* and *Parabacteroides* (p < 0.05). The total SCFA had negative correlations with *Bacteroides*, *[Prevotella]*, *[Ruminococcus]* and *Parabacteroides*, but was positively correlated with the abundance of *Lactobacillus* (p < 0.05).

4. Discussion

Ginseng is a medicinal-food homologous plant widely used in healthy food and healthcare products. Researchers have invented ginseng supplements with antioxidant, anti-inflammatory, fatigue-reducing and body-enhancing properties (Bach et al., 2016; J. Wang et al., 2022). Ginsenosides are important bioactive components. It is worth noting that the chemical structure of ginsenosides is likely to be the major factor influencing antioxidant and anti-inflammatory activities (W. Xu et al., 2023). Therefore, considerable efforts have been made to enhance the bioactivity of ginsenosides using various transformation methods such as physical, chemical and biological methods. Among these methods, the physical transformation method is more favorable for factory application. Zhang et al. reported that the ginsenoside type and amount changed after commercial sterilizing (121 °C, 30 min), and the contents of minor ginsenosides significantly increased in heat-treated fresh ginseng pulp (J. Zhang et al., 2022). The chemical structure of ginsenosides may change during partial hydrolysis of sugar moieties and dehydration at C3, C6, or C20 after heat treatment (Park et al., 2015). In the present study, ginsenosides Rb1, Rb2, Rb3, Rd and Re contents were significantly decreased by 61, 188, 203, 11 and 27

times, respectively, while the contents of the rare ginsenosides Rg3, Rh2 and Rg5 significantly were increased by 7, 106 and 70 times after heat treatment, respectively. Compared with the fresh ginseng, the contents of Rb1 and Rd in red ginseng increased 1–3 times, the contents of Rb2, Rb3, and Rc decreased 1–2 times, and the contents of rare ginsenosides Rh1 and Rh2 increased 1–2 times (H. Wang et al., 2023). The contents of ginsenosides Rg3 and Rh2 in black ginseng increased by 12 fold and 3 fold, respectively (Huang et al., 2023). Red ginseng and black ginseng are processed under complicated conditions and are not easy to consume. The heat treatment conditions (135 °C, 30 min, 60 mM citric acid) used in this study not only simplified the production process, but also significantly increased the content of rare ginsenosides. Moreover, new rare ginsenosides were generated, such as ginsenosides Rk2 and Rh3. The modes and pathways of transformation between ginsenosides under heat and acid treatments were summarized in Fig. 1B and C. In the pathway, Rb1, Rb2, Rb3 and Rc are converted to Rd by removing different types of sugar moieties at C20, after which Rd can continue to be converted to Rg3, Rg5 and Rk1 via deglycosylation and dehydration at C3 or C20. Rk2 is produced by deglycosylation of Rk1 at C3 and by deglycosylation and dehydration of Rg3 at C3 and C20. Rh3 is converted from Rh2 via dehydration at C20. Re is converted to Rg1 and Rg2 by removing different types of sugar moieties at C6 or C20, then Rg1 and Rg2 are converted to Rh1 and F1 via deglycosylation and dehydration at C6 or C20. Subsequently, the effects of the total ginsenosides from heat-treated fresh ginseng on CTX-induced liver injury were further analyzed.

CTX is a first-line anticancer drug and immunosuppressant, but it is harmful to the liver itself and other body tissues. However, the use of CTX is unavoidable, as there are still no clinically approved safe alternatives to CTX (Ahlmann and Hempel, 2016). Therefore, this study aimed to utilize ginsenosides to alleviate liver injury induced by CTX. In this study, CTX-treated mice exhibited significant anorexic behavior, with significant decreases in body weight and food intake (Fig. 2B and C), consistent with the symptoms observed in patients receiving chemotherapy. The surface of the CTX-treated liver was white and swollen with dense porosity, and H&E staining also showed extensive hepatocyte damage in the MC group mice (Fig. 3A and B). These

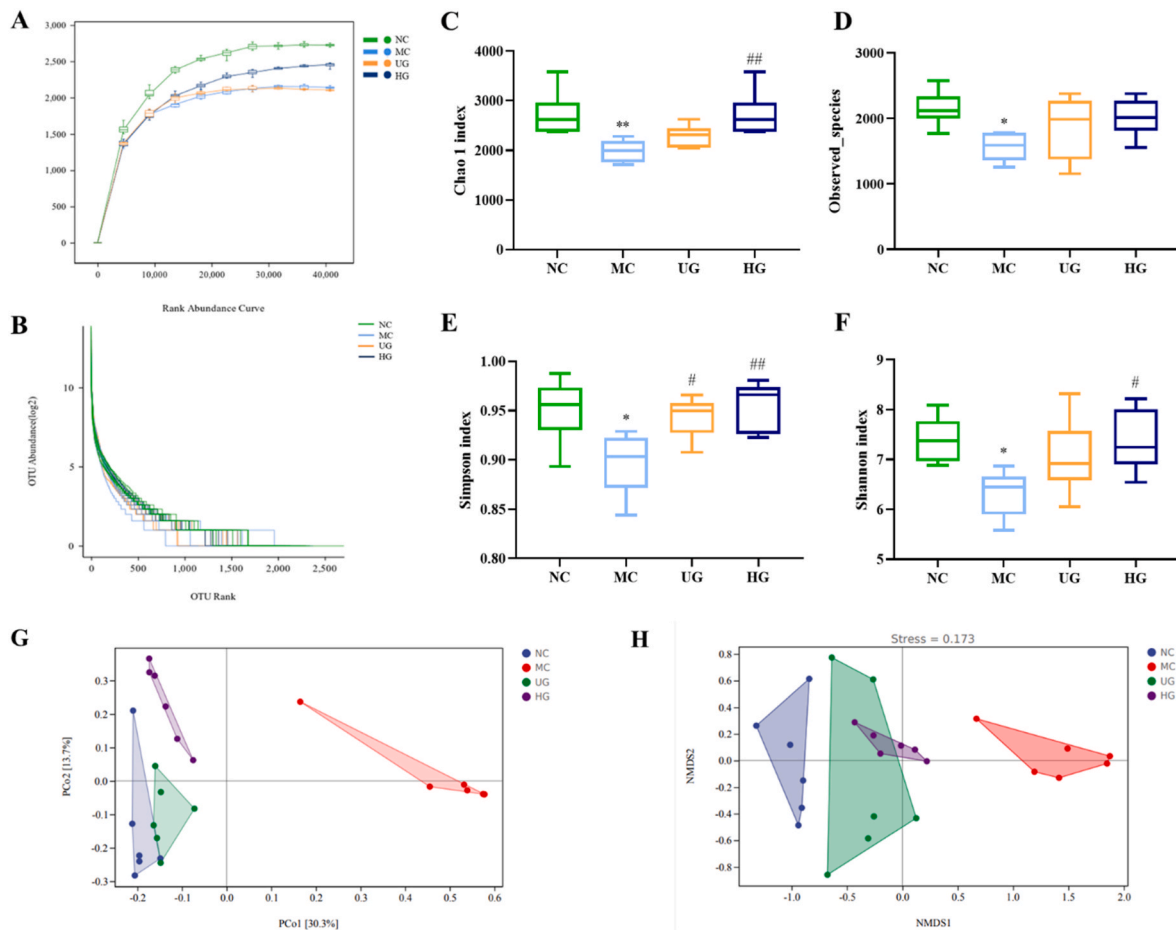


Fig. 6. Alpha and beta diversity of the intestinal microbiota. (A) The rarefaction curve; (B) The abundance rank curve; (C) Chao 1 index; (D) Observed species; (E) Simpson index; (F) Shannon index; (G) PCoA analysis; (H) NMDS analysis. Each point represents a sample, and different colored points belong to different groups. Data were shown as mean \pm SD ($n = 6$). (* $p < 0.05$), (** $p < 0.01$) as compared to the NC group. (# $p < 0.05$), (## $p < 0.01$) as compared to the MC group.

phenomena were also observed in earlier studies (N. Zhang et al., 2022). HG intervention significantly decreased liver index and ALT and AST levels in the serum and liver (Figs. 2D, 3C–F). UG and HG ameliorated the CTX-induced liver injury in a manner similar to that of lutein, pyrroloquinoline quinone, escin and allicin (Cengiz et al., 2022; El-Kholly et al., 2017; L. Qian et al., 2022; Sun et al., 2021).

Acrolein, a metabolite of CTX in vivo, can deplete cellular GSH, leading to GSH-dependent impairment of the antioxidant system and related apoptosis (Mohammed et al., 2020). Therefore, inhibiting oxidative reactions and up-regulating antioxidant molecules are key strategies for attenuating CTX-induced liver injury. HG intervention significantly increased the levels of GSH and T-SOD, while the effect of UG intervention was not significant (Fig. 4B–D). These results suggested that HG can effectively restore redox homeostasis in damaged liver by preventing GSH depletion induced by CTX and enhancing the activities of antioxidant enzymes. Moreover, many enzymes related to GSH synthesis and metabolism are under the control of Nrf2 (J. Liu et al., 2023). Nrf2 is closely associated with the production of antioxidant enzymes and cellular defense (Sun et al., 2021). When CTX enters the body to induce oxidative stress, Nrf2 can bind to ARE to form a heterodimer and initiate the transcription of genes coding for detoxification enzymes and antioxidants such as the downstream protein HO-1, activating the antioxidant defense system (Sherif, 2018). HG promoted the expression of hepatic Nrf2/HO-1 signaling pathway compared to MC group mice (Fig. 4E), which inhibited CTX-induced oxidative damage and enhanced the antioxidant defense of mice liver (Z. Zhang et al., 2021).

CTX attacks hepatocytes and leads to constant production of pro-inflammatory cytokines by immune cells, such as TNF- α . In the

present study, HG treatment decreased significantly in TNF- α levels in serum, while UG intervention had no significant effect (Fig. 5B–D). The TLR4 signaling pathway is implicated in the production of pro-inflammatory cytokines and activation of TLR4 stimulates the expression of a variety of signals, such as the MAPK pathway. Previous studies demonstrated that Mesona chinensis Benth polysaccharides protected against CTX-induced liver injury in mice via MAPKs signaling pathway (Huang et al., 2020). Another study demonstrated that Cyclocarya paliurus polysaccharide attenuated hepatic inflammation in CCl₄-induced mice by inhibiting the TLR4/MAPK pathway (Wu et al., 2020). These findings suggest that down-regulating TLR4/MAPK expression is an effective approach to alleviate liver inflammation. In this study, the expression of TLR4/MAPK was suppressed in the livers of mice by UG and HG (Fig. 5E). The results indicated that HG relieved CTX-induced hepatic inflammation by down-regulating the expression of the TLR4/MAPK pathway and reducing the release of TNF- α . Furthermore, overexpression of the MAPKs pathway inhibits its downstream Nrf2/HO-1 pathway (N. Zhang et al., 2022). HG intervention suppressed the CTX-induced oxidative stress by suppressing the MAPKs pathway and promoting the expression of Nrf2 and HO-1 proteins.

A growing number of research indicate that the gut flora and gut-derived products play a role in the pathogenesis of liver disease (Yip et al., 2018). In general, the normal intestinal flora is a natural barrier, and CTX treatment causes overgrowth of gram-negative bacteria and damage to the intestinal barrier, which leads to intestinal endotoxin (such as LPS) translocation (Q. Xu et al., 2022). LPS is a toxic metabolite of intestinal bacteria that can enter liver tissue through the portal vein and bind to its specific recognition receptor TLR4 to induce a series of

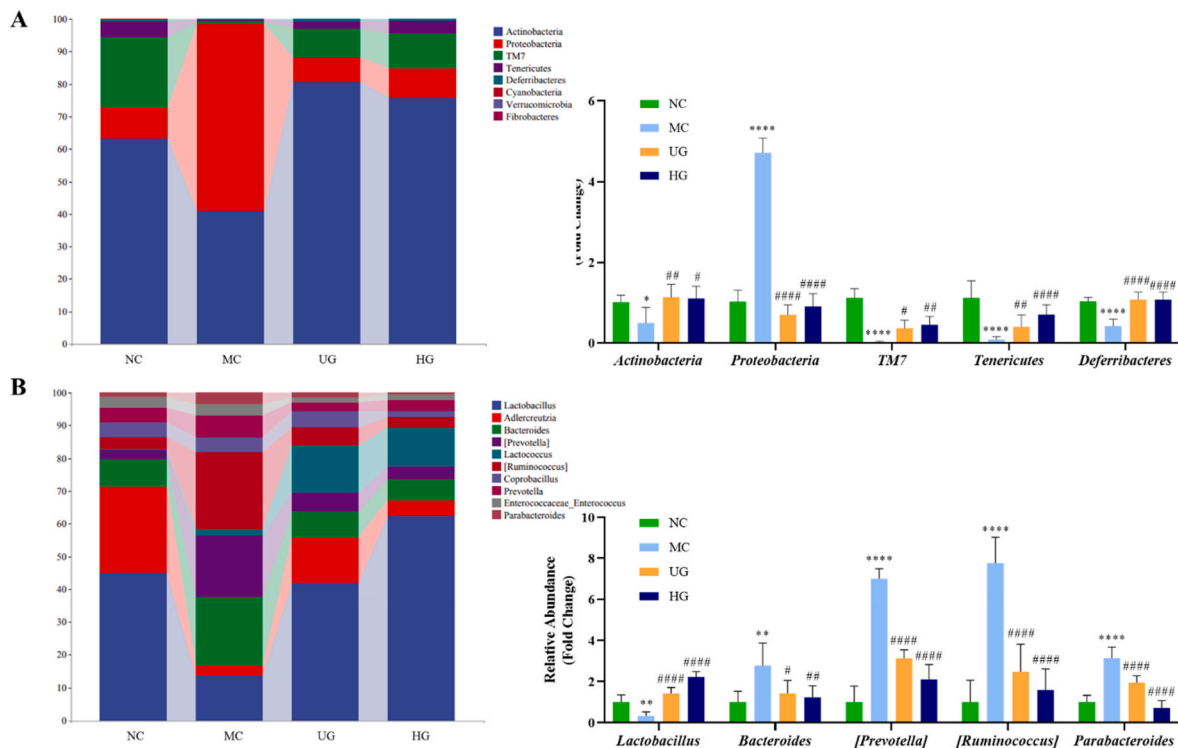


Fig. 7. Effect of HG on the gut microbiota composition in mice induced by CTX. (A) Gut microbiota composition at the phylum level; (B) gut microbiota composition at the genus level. Data were shown as mean ± SD (n = 6). (**p < 0.01), (***)p < 0.001) and (****p < 0.0001) as compared to the NC group. (#p < 0.05), (##p < 0.01), (###p < 0.001) and (####p < 0.0001) as compared to the MC group.

Table 1
The concentrations of SCFAs in the mice feces of different treatment groups.

Group	NC	MC	UG	HG
Acetic acid (µg/g)	1116.72 ± 252.1	510.23 ± 59.82*	1119.77 ± 90.58#	1269.10 ± 165.63##
Propionic acid (µg/g)	197.35 ± 3.58	131.79 ± 24.15	248.38 ± 24.28#	295.72 ± 40.01###
Butyric acid (µg/g)	372.28 ± 47.16	141.10 ± 9.94**	394.76 ± 20.70##	432.97 ± 67.92###
Isobutyric acid (µg/g)	23.62 ± 8.41	14.75 ± 3.17	18.09 ± 4.34	20.97 ± 6.22
Valeric acid (µg/g)	48.51 ± 9.83	17.25 ± 3.66**	38.00 ± 8.20	39.89 ± 4.81
Total SCFAs (µg/g)	1792.49 ± 317.71	852.32 ± 33.69*	1811.01 ± 195.39#	2048.44 ± 430.04#

Data were shown as mean ± SD (n = 6). (*p < 0.05), (**p < 0.01) as compared to the NC group. #p < 0.05, (##p < 0.01), (###p < 0.001) as compared to the MC group.

inflammatory cascade reactions, ultimately leading to liver inflammation and damage (Q. Xu et al., 2022). In the present study, UG and HG significantly inhibited the release of LPS into the liver and the TLR4/MAPK signaling pathway, and HG had a more significant effect (Fig. 5). However, the exact mechanism which UG and HG alleviate inflammation induced by LPS remains unclear.

Imbalance of intestinal flora can lead to altered immune responses and is linked to a broad range of liver diseases such as drug-induced liver injury, liver fibrosis and non-alcoholic fatty liver disease (NAFLD) (Matsuoka and Kanai, 2015). Here, alpha diversity analysis revealed that UG and HG intake promoted an increase in the diversity and richness of the gut microbiota, and the effect of HG was more significant (Fig. 6C–F). Similarly, beta diversity analysis showed a significant separation of the MC group mice from the NC group mice. The HG intervention group significantly deviated from the MC group and closed the NC group, suggesting that HG beneficially regulated the gut microbiota

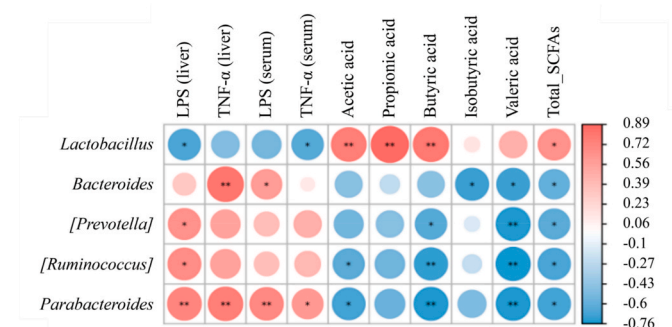


Fig. 8. Heatmap of Spearman correlation analysis between the key gut microbial taxa at the genus level and indicators associated with liver injury. The legend shows the value of the correlation coefficient, with colors ranging from blue (negative correlation) to red (positive correlation), with a significant correlation indicated by *p < 0.05 and **p < 0.01.

(Fig. 6G–H). At the phylum level, CTX treatment significantly promoted the growth of *Proteobacteria*. *Proteobacteria* are gram-negative bacteria that promote the production of LPS and participate in inflammatory processes, which can lead to ecological dysregulation of the intestinal flora and liver injury (Ying et al., 2020). However, the growth of *Proteobacteria* was inhibited by HG intervention. *Deferritibacteres* is known for the ability to reduce iron and other metals, this process involves transferring electrons from iron to bacteria, which can then use those electrons to produce energy to help keep the balance of iron and other metals in the ecosystem (Y. Li et al., 2019). In this study, HG intervention significantly increased the abundance of *Deferritibacteres*. Moreover, HG significantly promoted the growth of the beneficial bacteria *TM7* and *Tenericutes*, which is comparable to the results of previous studies (Fig. 7A) (Wu et al., 2020).

At the genus level, *Lactobacillus* is one of the most recognized

probiotics, and is considered to be the main source of SCFA production (Pan et al., 2023). A high level of *Lactobacillus* can stimulate immune cells, control gastrointestinal infections, modulate cytokine production, and alleviate inflammation by stimulating the TLR4/MAPK signaling pathways (Lv et al., 2021). C-phycocyanin intervention reversed the CTX-induced significant reduction in *Lactobacillus* and SCFAs such as acetic acid, propionic acid and butyric acid (X. Li et al., 2023). HG intervention increased the abundance of *Lactobacillus* compared to that in the MC group, which was consistent with the previously observed increase in the production of SCFAs. Moreover, Spearman's correlation analysis also confirmed the above result (Fig. 8). Both *Bacteroides* and *Prevotella* are gram-negative bacteria, and LPS is secreted by these bacteria (Sharma et al., 2022; L. Zhang et al., 2019). This study revealed that CTX treatment significantly increased the abundance of *Bacteroides* and *Prevotella*, which corresponded to the increase in LPS content (Fig. 5A–C). Fortunately, HG intervention reversed these changes. *Parabacteroides* is a unique bacterium associated with chronic metabolic diseases and oxidative stress (Ezeji et al., 2021). Its abundance positively correlates with inflammatory markers and promotes inflammation (Wan et al., 2022), which is consistent with the results of our Spearman correlation analysis (Fig. 8). In addition, *Ruminococcus* is recognized as a bacterium associated with gastrointestinal diseases (L. Wang et al., 2013). Our results showed that CTX intervention significantly increased the relative abundance of *Parabacteroides* and *Ruminococcus*. However, UG and HG intervention effectively inhibited the production of these two pathogenic bacteria, and the effect of HG was more significant (Fig. 7B). The above results suggested that HG can alter the composition of the intestinal flora by promoting the growth of SCFA-producing bacteria and inhibiting the expansion of LPS-producing bacteria. These findings directly suggest that the process of attenuating CTX-induced hepatic injury by HG is closely linked to the modulation of the intestinal flora.

SCFAs can regulate pro- and anti-inflammatory processes in vivo through multiple pathways with a wide range of host health benefits (Yang et al., 2024). SCFAs prevent LPS from entering the bloodstream through the intestinal mucosa and damaging the liver (Hu et al., 2013). SCFAs mainly include acetic acid, propionic acid and butyric acid. In particular, acetic acid and propionic acid can modulate neutrophil activation and reduce the inflammatory cascade by inhibiting cytokine expression (Z. Wang et al., 2020). Propionic acid can also directly affect hepatic metabolism (Shi et al., 2017). In addition, butyric acid can inhibit inflammatory factor expression and reduce TLR4 activation, thereby reducing intestinal inflammatory responses (Shi et al., 2017). CTX significantly suppressed the concentrations of acetic, propionic, butyric, and valeric acids in mice feces (Wu et al., 2020; Z. Zhang et al., 2020). Several studies have shown that polysaccharides, purple-red rice anthocyanins, and natural *Cordyceps sinensis* ameliorated CTX-induced side effects or liver injury by modulating SCFAs (Chen et al., 2022; Fang et al., 2021; Z. Zhang et al., 2020). In this study, CTX induced a significant decrease in several SCFAs. Fortunately, HG effectively protected the gut and liver by promoting the production of SCFAs (Table 1).

5. Conclusion

Fresh ginseng heated at high temperature in the presence of citric acid significantly promoted the conversion of major ginsenosides into rare ginsenosides, and the effect of heat-treated fresh ginseng total ginsenosides on alleviating CTX-induced liver injury was significantly enhanced. HG ameliorated CTX-induced liver injury by affecting the composition of the intestinal flora, promoting the production of SCFAs, and suppressing the enterohepatic LPS-TLR4-MAPK signaling pathway. These results support the view that targeting the intestinal microbiota may be an emerging strategy for mitigating CTX-induced liver injury. These findings provide new perspectives on the application of fresh ginseng and the wellness effects of HG as a functional food ingredient.

Ethics statement

All experimental procedures concerning animals and their caring were authorized by the Animal Ethics Committee of Jilin Agricultural University (No. 20190410005).

CRediT authorship contribution statement

Ping Tang: Investigation, Writing – original draft, Visualization, Data curation. **Guangquan Ren:** Investigation, Writing – original draft, Visualization, Data curation. **Hongyang Zou:** Investigation, Software. **Sitong Liu:** Writing – review & editing. **Junshun Zhang:** Writing – review & editing. **Zhiyi Ai:** Software. **Yue Hu:** Software. **Linlin Cui:** Software. **Bo Nan:** Writing – review & editing. **Zhicheng Zhang:** Validation, Resources, Writing – review & editing, Supervision. **Yuhua Wang:** Validation, Resources, Writing – review & editing, Supervision.

Declaration of competing interest

The authors declare that they have no known competing financial interests or personal relationships that could have appeared to influence the work reported in this paper.

Data availability

Data will be made available on request.

Acknowledgements

This work was supported by the Key R&D Program of Jilin Provincial Department of Science and Technology (20210204040YY).

Appendix A. Supplementary data

Supplementary data to this article can be found online at <https://doi.org/10.1016/j.crfs.2024.100734>.

References

- Abdelfattah-Hassan, A., Shalaby, S.I., Khater, S.I., El-Shetry, E.S., Abd El Fadil, H., Elsayed, S.A., 2019. Panax ginseng is superior to vitamin E as a hepatoprotector against cyclophosphamide-induced liver damage. *Compl. Ther. Med.* 46, 95–102. <https://doi.org/10.1016/j.ctim.2019.08.005>.
- Ahlmann, M., Hempel, G., 2016. The effect of cyclophosphamide on the immune system: implications for clinical cancer therapy. *Cancer Chemother. Pharmacol.* 78 (4), 1–11. <https://doi.org/10.1007/s00280-016-3152-1>.
- Bach, H.V., Kim, J., Myung, S.K., Cho, Y.A., 2016. Efficacy of ginseng supplements on fatigue and physical performance: a meta-analysis. *J. Kor. Med. Sci.* 31 (12), 1879–1886. <https://doi.org/10.3346/jkms.2016.31.12.1879>.
- Cengiz, M., Kutlu, H.M., Peker Cengiz, B., Ayhan, A., 2022. Escin attenuates oxidative damage, apoptosis and lipid peroxidation in a model of cyclophosphamide-induced liver damage. *Drug Chem. Toxicol.* 45 (3), 1180–1187. <https://doi.org/10.1080/01480545.2020.1810262>.
- Chen, T., Shen, M., Yu, Q., Chen, Y., Wen, H., Lu, H., Chen, S., Xie, J., 2022. Purple red rice anthocyanins alleviate intestinal damage in cyclophosphamide-induced mice associated with modulation of intestinal barrier function and gut microbiota. *Food Chem.* 397, 133768. <https://doi.org/10.1016/j.foodchem.2022.133768>.
- El-Kholy, A.A., Elkablawy, M.A., El-Agamy, D.S., 2017. Lutein mitigates cyclophosphamide induced lung and liver injury via NF- κ B/MAPK dependent mechanism. *Biomedicine & Pharmacotherapy = Biomedecine & Pharmacotherapie* 92, 519–527. <https://doi.org/10.1016/j.biopha.2017.05.103>.
- Ezeji, J.C., Sarikonda, D.K., Hopperton, A., Erkkila, H.L., Cohen, D.E., Martinez, S.P., Cominelli, F., Kuwahara, T., Dichosa, A.E.K., Good, C.E., Jacobs, M.R., Khoretchenko, M., Veloo, A., Rodriguez-Palacios, A., 2021. Parabacteroides distansoni: intriguing aerotolerant gut anaerobe with emerging antimicrobial resistance and pathogenic and probiotic roles in human health. *Gut Microb.* 13 (1), 1922241. <https://doi.org/10.1080/19490976.2021.1922241>.
- Fang, Q., Chen, S., Wang, J., Huang, X., Nie, Q., Phillips, G.O., Cui, S.W., Li, Y., Nie, S., 2021. Fractions from natural *Cordyceps sinensis* alleviated intestinal injury in cyclophosphamide-induced mice. *Bioactive Carbohydrates and Dietary Fibre* 26, 100271. <https://doi.org/10.1016/j.bcdf.2021.100271>.
- Gao, Y., Yan, J., Li, J., Li, X., Yang, S., Chen, N., Li, L., Zhang, L., 2021. Ginsenoside Rg3 ameliorates acetaminophen-induced hepatotoxicity by suppressing inflammation

- and oxidative stress. *J. Pharm. Pharmacol.* 73 (3), 322–331. <https://doi.org/10.1093/jpp/rgaa069>.
- Guo, M., Zhu, C., Fu, R., Ma, X., Duan, Z., Fan, D., 2023. Ginsenoside Rk3 regulates nonalcoholic steatohepatitis by modulation of intestinal flora and the PI3K/AKT signaling pathway in C57BL/6 mice. *J. Agric. Food Chem.* 71 (24), 9370–9380. <https://doi.org/10.1021/acs.jafc.3c00789>.
- Hong, Y., Shen, M., Huang, L., Wu, T., Xie, J., 2022. Mesona chinensis Benth polysaccharides alleviates liver injury by beneficial regulation of gut microbiota in cyclophosphamide-induced mice. *Food Sci. Hum. Wellness* 11 (1), 74–84. <https://doi.org/10.1016/j.fshw.2021.07.009>.
- Hu, J.L., Nie, S.P., Li, H., Xie, M.Y., 2013. In vitro fermentation of polysaccharide from the seeds of *Plantago asiatica* L by human fecal microbiota. *Food Hydrocolloids* 33, 384–392. <https://xueshu.baidu.com/usercenter/paper/show?paperid=851592a08d2b4260e72174b33299fd8&site=xueshu.se>.
- Huang, L., Li, H.-J., Wu, Y.-C., 2023. Processing technologies, phytochemistry, bioactivities and applications of black ginseng—a novel manufactured ginseng product: a comprehensive review. *Food Chem.* 407, 134714 <https://doi.org/10.1016/j.foodchem.2022.134714>.
- Huang, L., Shen, M., Wu, T., Yu, Y., Yu, Q., Chen, Y., Xie, J., 2020. Mesona chinensis Benth polysaccharides protect against oxidative stress and immunosuppression in cyclophosphamide-treated mice via MAPKs signal transduction pathways. *Int. J. Biol. Macromol.* 152, 766–774. <https://doi.org/10.1016/j.ijbiomac.2020.02.318>.
- J, C., Z, L., M, H., Y, S., 2021. Protection by ginseng saponins against cyclophosphamide-induced liver injuries in rats by induction of cytochrome P450 expression and mediation of the l-arginine/nitric oxide pathway based on metabolomics. *Phytother. Res.* 35 (6), 6951. <https://doi.org/10.1002/ptr.6951>.
- Li, K., Wang, L., Zhou, R., Fan, H., Sui, J., 2019. Amelioration of alcohol-induced liver injury in mice by ginsenosides in ginseng wine. *J. Funct. Foods* 54, 281–288. <https://doi.org/10.1016/j.jff.2019.01.014>.
- Li, X., Zhao, M., Ding, Z., Wang, X., Zhang, Z., 2023. C-phycocyanin ameliorates cyclophosphamide-induced liver injury and metabolic disorder through the modulation of the gut microbiota in mice. *Algal Res.* 71, 103093 <https://doi.org/10.1016/j.algal.2023.103093>.
- Li, Y., Luan, Y., Yue, X., Xiang, F., Mao, D., Cao, Y., Xiong, Z., 2019. Effects of Codonopsis bulleyana forest ex diols on *Deferribacteres* in constipation predominant intestine tumor: differential analysis. *Saudi J. Biol. Sci.* 26 (2), 395–401. <https://doi.org/10.1016/j.sjbs.2018.11.008>.
- Liu, J., Yang, G., Zhang, H., 2023. Glyphosate-triggered hepatocyte ferroptosis via suppressing Nrf2/GSH/GPX4 axis exacerbates hepatotoxicity. *Sci. Total Environ.* 862, 160839 <https://doi.org/10.1016/j.scitotenv.2022.160839>.
- Liu, R., Gao, Y., Yuan, Y., Wu, Q., Zhi, Z., Muhindo, E.M., Wu, T., Sui, W., Zhang, M., 2022. Transformation of ginsenosides by moderate heat-moisture treatment and their cytotoxicity toward HepG2 cells. *Food Res. Int.* 156, 111155 <https://doi.org/10.1016/j.foodres.2022.111155>.
- Lv, L., Mu, D., Du, Y., Yan, R., Jiang, H., 2021. Mechanism of the Immunomodulatory effect of the combination of live bifidobacterium, *Lactobacillus*, *Enterococcus*, and *Bacillus* on immunocompromised rats. *Front. Immunol.* 12, 694344 <https://doi.org/10.3389/fimmu.2021.694344>.
- Matsuo, K., Kanai, T., 2015. The gut microbiota and inflammatory bowel disease. *Semin. Immunopathol.* 37 (1), 47–55. <https://doi.org/10.1007/s00281-014-0454-4>.
- Mohammed, M.J., Tadros, M.G., Michel, H.E., 2020. Geraniol protects against cyclophosphamide-induced hepatotoxicity in rats: possible role of MAPK and PPAR- γ signaling pathways. *Food Chem. Toxicol.: An International Journal Published for the British Industrial Biological Research Association* 139, 111251. <https://doi.org/10.1016/j.fct.2020.111251>.
- Ms, S., Jh, S., P, C., Jh, L., Sy, K., Ks, S., J, H., Ks, K., 2018. Stimulation of innate immune function by Panax ginseng after heat processing. *J. Agric. Food Chem.* 66 (18) <https://doi.org/10.1021/acs.jafc.8b00152>.
- Pan, L.-L., Ren, Z.-N., Yang, J., Li, B.-B., Huang, Y.-W., Song, D.-X., Li, X., Xu, J.-J., Bhatia, M., Zou, D.-W., Zhou, C.-H., Sun, J., 2023. Gut microbiota controls the development of chronic pancreatitis: a critical role of short-chain fatty acids-producing Gram-positive bacteria. *Acta Pharm. Sin. B* 13 (10), 4202–4216. <https://doi.org/10.1016/j.apsb.2023.08.002>.
- Park, J.Y., Choi, P., Kim, T., Ko, H., Kim, H., Kang, K.S., Ham, J., 2015. Protective effects of processed ginseng and its active ginsenosides on cisplatin-induced nephrotoxicity: in vitro and in vivo studies. *J. Agric. Food Chem.* 63 (25), 5964–5969. <https://doi.org/10.1021/acs.jafc.5b00782>.
- Patwa, J., Khan, S., Jena, G., 2020. Nicotinamide attenuates cyclophosphamide-induced hepatotoxicity in SD rats by reducing oxidative stress and apoptosis. *J. Biochem. Mol. Toxicol.* 34 (10), e22558 <https://doi.org/10.1002/jbt.22558>.
- Qian, L., Yang, F., Lin, X., Jiang, S., Zhang, Y., Tang, Y., 2022. Pyrroloquinoline quinone ameliorates liver injury in mice induced by cyclophosphamide. *Environ. Sci. Pollut. Res. Int.* 29 (20), 30383–30393. <https://doi.org/10.1007/s11356-021-17990-6>.
- Qian, Y., Huang, R., Li, S., Xie, R., Qian, B., Zhang, Z., Li, L., Wang, B., Tian, C., Yang, J., Xiang, M., 2019. Ginsenoside Rh2 reverses cyclophosphamide-induced immune deficiency by regulating fatty acid metabolism. *J. Leukoc. Biol.* 106 (5), 1089–1100. <https://doi.org/10.1002/JLB.2A0419-117R>.
- Sharma, G., Garg, N., Hasan, S., Shirodkar, S., 2022. Prevotella: an insight into its characteristics and associated virulence factors. *Microb. Pathog.* 169, 105673 <https://doi.org/10.1016/j.micpath.2022.105673>.
- Sherif, I.O., 2018. The effect of natural antioxidants in cyclophosphamide-induced hepatotoxicity: role of Nrf2/HO-1 pathway. *Int. Immunopharm.* 61, 29–36. <https://doi.org/10.1016/j.intimp.2018.05.007>.
- Shi, H., Chang, Y., Gao, Y., Wang, X., Chen, X., Wang, Y., Xue, C., Tang, Q., 2017. Dietary fucoidan of *Acaudina molpadioides* alters gut microbiota and mitigates intestinal mucosal injury induced by cyclophosphamide. *Food Funct.* 8 (9), 3383–3393. <https://doi.org/10.1039/c7fo00932a>.
- Song, X., Gao, W., Shi, Y., Li, J., Zheng, Z., 2023. Panax ginseng and its derivatives: promoting angiogenesis in ischemic diseases – a mechanistic overview. *J. Funct. Foods* 109, 105762. <https://doi.org/10.1016/j.jff.2023.105762>.
- Su, Y., Cheng, S., Ding, Y., Wang, L., Sun, M., Man, C., Zhang, Y., Jiang, Y., 2023. A comparison of study on intestinal barrier protection of polysaccharides from *Hericium erinaceus* before and after fermentation. *Int. J. Biol. Macromol.* 233, 123558 <https://doi.org/10.1016/j.ijbiomac.2023.123558>.
- Sun, D., Sun, C., Qiu, G., Yao, L., Yu, J., Al Sberi, H., Fouda, M.S., Othman, M.S., Lokman, M.S., Kassab, R.B., Abdel Moneim, A.E., 2021. Allicin mitigates hepatic injury following cyclophosphamide administration via activation of Nrf2/ARE pathways and through inhibition of inflammatory and apoptotic machinery. *Environ. Sci. Pollut. Res. Int.* 28 (29), 39625–39636. <https://doi.org/10.1007/s11356-021-13392-w>.
- Wan, Y., Yang, L., Li, H., Ren, H., Zhu, K., Dong, Z., Jiang, S., Shang, E., Qian, D., Duan, J., 2022. Zingiber officinale and Panax ginseng ameliorate ulcerative colitis in mice via modulating gut microbiota and its metabolites. *J. Chromatogr. B* 1203, 123313. <https://doi.org/10.1016/j.jchromb.2022.123313>.
- Wang, H., Cheng, Y., Zhang, X., Wang, Y., Zhao, H., 2023. Comparative analysis of physicochemical properties, ginsenosides content and α -amylase inhibitory effects in white ginseng and red ginseng. *Food Sci. Hum. Wellness* 12 (1), 14–27. <https://doi.org/10.1016/j.fshw.2022.07.014>.
- Wang, J., Zeng, L., Zhang, Y., Qi, W., Wang, Z., Tian, L., Zhao, D., Wu, Q., Li, X., Wang, T., 2022. Pharmacological properties, molecular mechanisms and therapeutic potential of ginsenoside Rg3 as an antioxidant and anti-inflammatory agent. *Front. Pharmacol.* 13, 975784 <https://doi.org/10.3389/fphar.2022.975784>.
- Wang, L., Christophersen, C.T., Soric, M.J., Gerber, J.P., Angley, M.T., Conlon, M.A., 2013. Increased abundance of *Sutterella* spp. and *Ruminococcus torques* in feces of children with autism spectrum disorder. *Mol. Autism* 4, 42. <https://doi.org/10.1186/2040-2392-4-42>.
- Wang, Z., Zhang, X., Zhu, L., Yang, X., He, F., Wang, T., Bao, T., Lu, H., Wang, H., Yang, S., 2020. Inulin alleviates inflammation of alcoholic liver disease via SCFAs-inducing suppression of M1 and facilitation of M2 macrophages in mice. *Int. Immunopharm.* 78, 106062 <https://doi.org/10.1016/j.intimp.2019.106062>.
- Wu, T., Shen, M., Guo, X., Huang, L., Yang, J., Yu, Q., Chen, Y., Xie, J., 2020. Cyclocarya paliurus polysaccharide alleviates liver inflammation in mice via beneficial regulation of gut microbiota and TLR4/MAPK signaling pathways. *Int. J. Biol. Macromol.* 160, 164–174. <https://doi.org/10.1016/j.ijbiomac.2020.05.187>.
- Xu, Q., Zhang, R., Mu, Y., Song, Y., Hao, N., Wei, Y., Wang, Q., Mackay, C.R., 2022. Propionate ameliorates alcohol-induced liver injury in mice via the gut–liver Axis: focus on the improvement of intestinal permeability. *J. Agric. Food Chem.* 70 (20), 6084–6096. <https://doi.org/10.1021/acs.jafc.2c00633>.
- Xu, W., Lyu, W., Duan, C., Ma, F., Li, X., Li, D., 2023. Preparation and bioactivity of the rare ginsenosides Rg3 and Rh2: an updated review. *Fitoterapia* 167, 105514. <https://doi.org/10.1016/j.fitote.2023.105514>.
- Xue, P., Yao, Y., Yang, X.-S., Feng, J., Ren, G.-X., 2017. Improved antimicrobial effect of ginseng extract by heat transformation. *Journal of Ginseng Research* 41 (2), 180–187. <https://doi.org/10.1016/j.jgr.2016.03.002>.
- Yang, F., Liu, C., Lu, X., Liu, S., Zhang, Y., Yu, Y., Long, Y., 2024. Cistanche deserticola improves postmenopausal osteoporosis through gut microbiota and short-chain fatty acids. *J. Funct. Foods* 112, 105925. <https://doi.org/10.1016/j.jff.2023.105925>.
- Ying, M., Yu, Q., Zheng, B., Wang, H., Wang, J., Chen, S., Nie, S., Xie, M., 2020. Cultured *Cordyceps sinensis* polysaccharides modulate intestinal mucosal immunity and gut microbiota in cyclophosphamide-treated mice. *Carbohydr. Polym.* 235, 115957 <https://doi.org/10.1016/j.carbpol.2020.115957>.
- Yip, L.Y., Aw, C.C., Lee, S.H., Hong, Y.S., Ku, H.C., Xu, W.H., Chan, J.M.X., Cheong, E.J. Y., Chng, K.R., Ng, A.H.Q., Nagarajan, N., Mahendran, R., Lee, Y.K., Browne, E.R., Chan, E.C.Y., 2018. The liver-gut microbiota axis modulates hepatotoxicity of tacrine in the rat (Baltimore, Md.). *Hepatology* 67 (1), 282–295. <https://doi.org/10.1002/hep.29327>.
- Zhang, J., Ai, Z., Hu, Y., Wang, Y., Liu, S., Liu, Y., Nan, B., Wang, Y., 2022. Remarkable impact of commercial sterilizing on ginsenosides transformation in fresh ginseng pulp based on widely targeted metabolomics analysis. *Food Chem. X* 15, 100415. <https://doi.org/10.1016/j.fochx.2022.100415>.
- Zhang, L., Wu, Y.-N., Chen, T., Ren, C.-H., Li, X., Liu, G.-X., 2019. Relationship between intestinal microbial dysbiosis and primary liver cancer. *Hepatobiliary Pancreat. Dis. Int.: HBPD INT* 18 (2), 149–157. <https://doi.org/10.1016/j.hbpd.2019.01.002>.
- Zhang, N., Tian, Y., Wang, Y., Fan, Y., Zhang, Y., Xing, X., Nan, B., Ai, Z., Li, X., Wang, Y., 2022. Ameliorative effect of *Lactobacillus plantarum* Lp2 against cyclophosphamide-induced liver injury in mice. *Food Chem. Toxicol.* 169, 113433 <https://doi.org/10.1016/j.fct.2022.113433>.
- Zhang, Z., Fan, S., Huang, D., Xiong, T., Nie, S., Xie, M., 2020. Polysaccharides from fermented *Asparagus officinalis* with *Lactobacillus plantarum* NCU116 alleviated liver injury via modulation of glutathione homeostasis, bile acid metabolism, and SCFA production. *Food Funct.* 11 (9), 7681–7695. <https://doi.org/10.1039/d0fo01435d>.
- Zhang, Z., Pan, T., Liu, C., Shan, X., Xu, Z., Hong, H., Lin, H., Chen, J., Sun, H., 2021. Cyclophosphamide induced physiological and biochemical changes in mice with an emphasis on sensitivity analysis. *Ecotoxicol. Environ. Saf.* 211, 111889 <https://doi.org/10.1016/j.ecoenv.2020.111889>.
- Zhao, Y., Yan, Y., Zhou, W., Chen, D., Cao, Y., 2020. Effects of polysaccharides from bee collected pollen of Chinese wolfberry on immune response and gut microbiota composition in cyclophosphamide-treated mice. *J. Funct. Foods* 72, 104057. <https://doi.org/10.1016/j.jff.2020.104057>.